LBID-2449
CBP Tech Note -271
November 25, 2002

Lattice for Berkeley Femtosecond X-ray Light Source

A.Zholents, D.Robin, J.Tanabe, W.Wan
Ernest Orlando Lawrence Berkeley National Laboratory
1 Cyclotron Road
Berkeley, California 94720, USA

E.Forest
KEK, Ibaraki-ken, Japan

D. Kairan,
Budker Institute for Nuclear Physics
630090 Novosibirsk, Russia

This work was supported by the U.S.Department of Energy under Contract No. DE-AC03-76SF00098.

Abstract

The lattice of the recirculating accelerator has been designed to meet all requirements for the femtosecond x-ray light source. The design permits tunability of the time-of-flight parameters, betatron phase advances, and chromaticity over the different sections of the lattice. The photon production section has been designed with six identical cells with variable beta-functions at the undulator and bend magnet x-ray source points. Tracking studies indicate that lattice design is insensitive to typical errors in magnetic field quality, but needs beam based alignment to correct for alignment errors.

1. Introduction

Berkeley Femtosecond X-ray Light Source [Ref.1] is a recirculating accelerator, where electrons are injected at a 120 MeV and reach their final energy of 2.5 GeV in four passes through a linear accelerator (linac). Figure 1 shows a layout of the main machine and injector. The machine core is a 600 MeV superconducting linac based on TESLA cryomodules [Ref.2]. Three magnetic arcs connect the end and the beginning of the linac and serve for a beam return to the linac for a next step of acceleration. The forth arc delivers the electron beam to an array of undulators and bend magnets in a photon production section. The beam goes into the dump after it passes the photon production section.

Minimizing the footprint of the accelerator imposes a major constrain on global machine parameters such as a shape and a circumference of the outer ring, length of a photon production section, and the length of the main linac. The circumferences of the three inner rings are less constrained, however, although they must be carefully selected to allow the machine to be used in the energy recovery mode and with a high electron beam current provided by operation with multiple bunches within the accelerator at any given time. In the case of multi-bunch operation to provide a high average flux, a uniform spacing of all electron bunches in the linac including accelerating and decelerating bunches is highly desirable. The set of ring circumferences given in Table 1

provides a wide variety of choices for a bunch repetition rate out of the gun, leading to almost uniform bunch spacing in the 1.3 GHz main linac. An extra half wavelength in ring 4 is needed in order to launch the returning electron beam into the decelerating phase of the rf field in the linac.

Table 1. Ring circumferences

Ring number	Circumference, m	Number of RF wavelengths
1	186.793762	810
2	205.473139	891
3	236.605432	1026
4	295.75679	1282.5

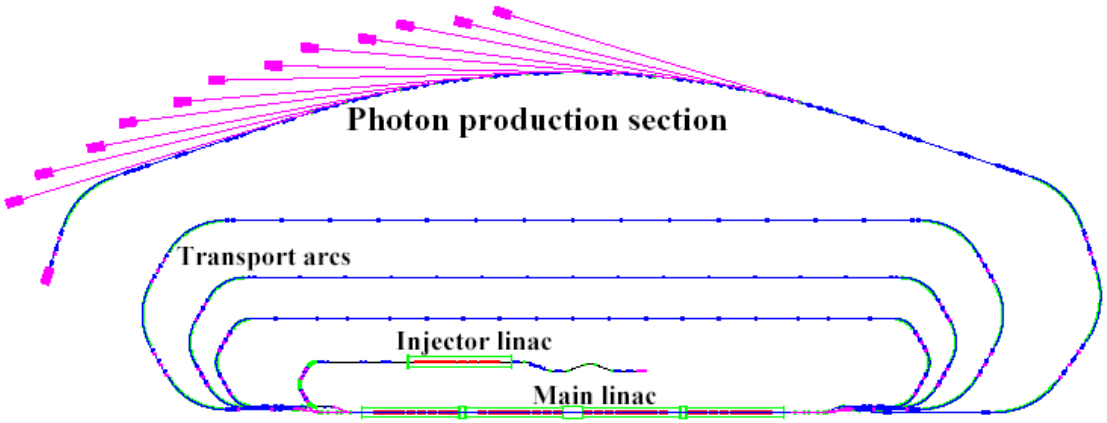

Figure 1. Machine layout, showing injector linac, main linac, four rings, and photon production section.

All four rings of the machine posses mirror symmetry relative to a central line dividing the machine into two halves. The presence of this symmetry simplifies the machine lattice and makes it acceptable for an acceleration and deceleration of electrons in the same linac. Although we do not plan now to decelerate the electrons, this possibility will be available for us when we will need it.

The lattice design allows the option to increase the electron beam energy in the photon production section from 2.5 GeV to 3.1 GeV, by increasing the energy gain in the main linac. This requires that the electron beam energy at the exit of the injector linac, and the magnetic strengths of all magnetic elements, will be simultaneously raised by the same factor.

2. Lattice description

Here we describe the accelerator lattice in different sections of the machine, a shorter version of this description is given in the reference [Ref 3]. With the exception of a few specialized magnets in the “beam combiner” or “beam spreader” sections which transport

the beams entering or exiting the main linac, all magnets are of a conventional electromagnet design similar to those of existing synchrotron radiation sources.

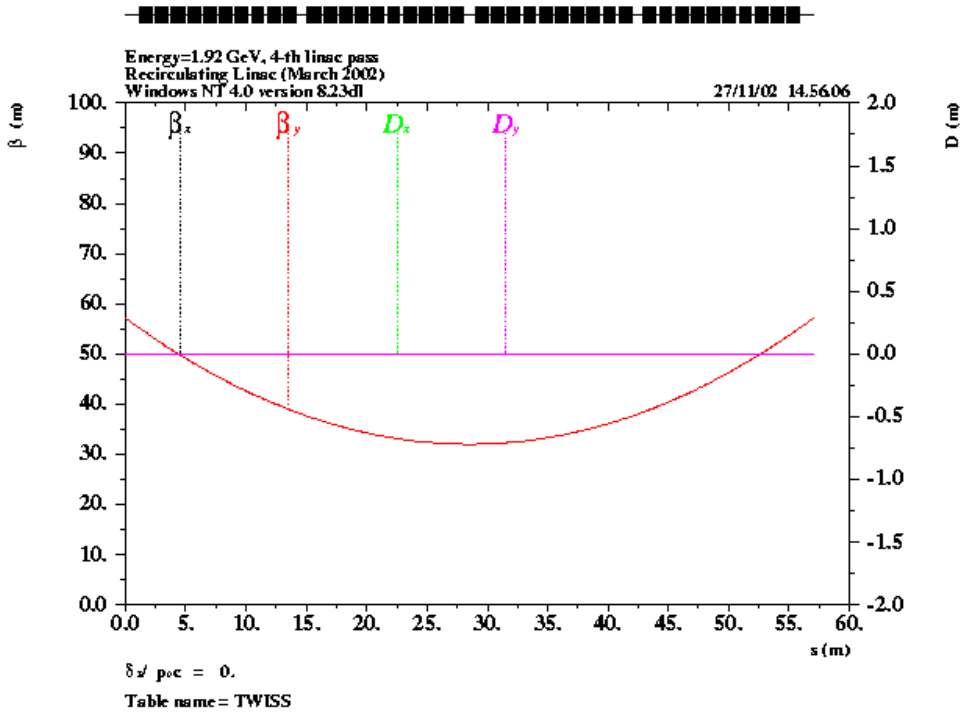

Figure 2. Beta-functions in the main linac.

2.1 Linac

Linac is the simplest part of the machine from a lattice point of view. Apart from a weak rf focusing that is only visible at electron beam energies below few hundred MeV it has no other beam focusing elements. Like in a drift space, linac beta-functions are freely expand towards both ends of the linac as shown in Figure 2. The only exclusion is the beginning of the first pass where beta-functions are constrained by the rf focusing (see, Figure 3.)

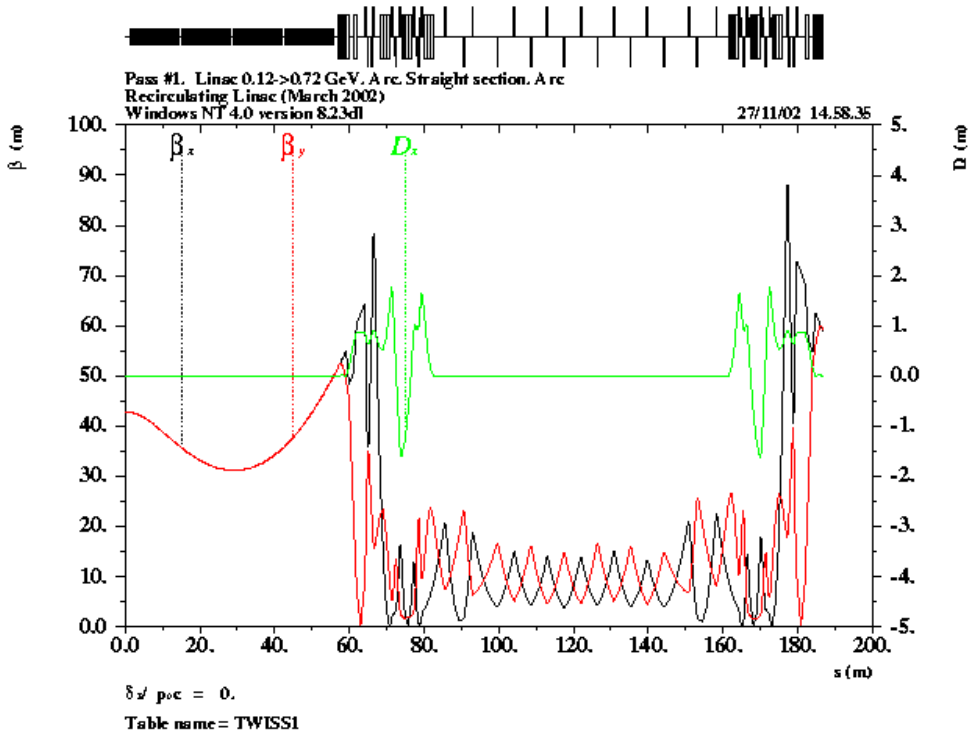

Figure 3. The lattice functions in the ring 1. The lattice of all other rings is very similar to this one except the beginning of the linac where effect of the RF focusing is visible.

2.2 Beam Spreader and Combiner

A *beam spreader* section (see, Figure 4) directs the electron beam at various energies after the linac into their respective rings. Its mirror image a *beam combiner* reconciles different energy orbits into a single line in the linac. This is a rather sophisticated part of the lattice because of the inevitable proximity of beamlines of different energies. The magnet B0 (with the field of 1.14 T and the length of 0.82 m) begins orbit separation. This is a rectangular magnet with the entrance and exit faces orthogonal to a linac line. It turns 720 MeV beam on 22.276°, 1.32 GeV beam on 11.933°, 1.92 GeV beam on 8.172°, and 2.52 GeV beam on 6.218°. Downstream magnets B1 and B2 have the same length as B0 and the same but opposite polarity magnetic field. They are also rectangular magnets with the entrance and exit faces positioned as the entrance and exit faces of B0. These magnets complete separation of different energy beams into the rings 1, 2, and 3 and constrain a *dispersion Courant-Snyder invariant* excited in B0. After B1 and B2 all orbits go parallel with the following separations between them: 175.7 mm between 720 MeV beam and 1.32 GeV beam, 188.4 mm between 1.32 GeV beam and 1.92 GeV beam, and 96.7 mm between 1.92 GeV beam and 2.52 GeV beam. The separation of the last two orbits is sufficient to give a room for a septum magnet B3 (see, Figure 5a) that has the same polarity as B2. This magnet affects only the orbit of 2.52 GeV beam and turns it away from the orbit of 1.92 GeV beam. Finally the magnet B4 completes the separation

of 2.52 GeV beam orbit. Four magnets B0, B2, B3 and B4 form a chicane with zero orbit displacement and zero dispersion at the end.

Besides bending magnets, there are four quadrupole lenses on each of the three lower energy beamlines and two quadrupole lenses on 2.52 GeV beamline. They are used for matching of the beta-functions in the linac to the beta-function of each of the respective arcs. Because of the tight orbit settings, quadrupole locations are carefully chosen so that they do not appear standing side by side. The mechanical design of these quadrupoles shown in Figure 5b is also compact in the horizontal plane. There are also two sextupoles on each of the beamlines. They are used to control chromaticity and T_{566} time-off-flight parameter.

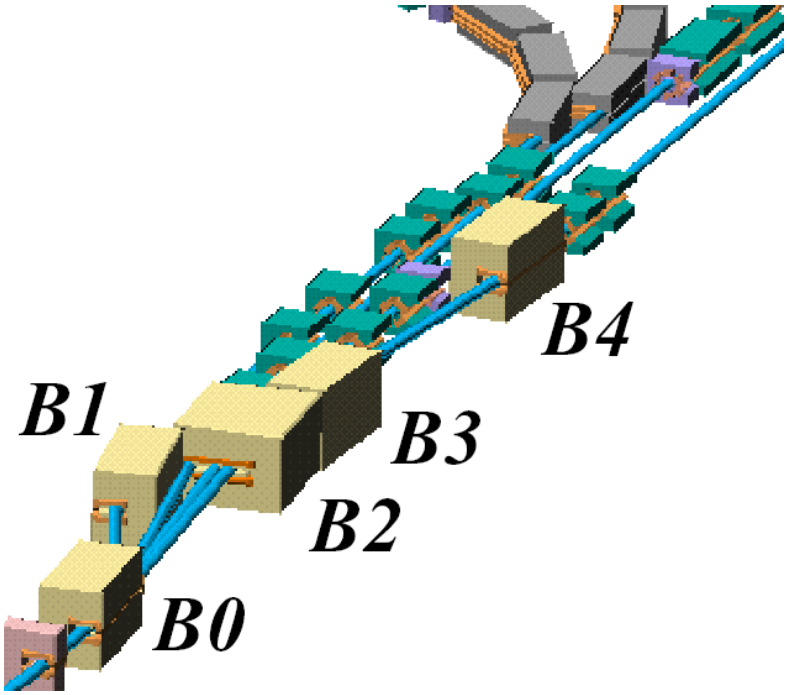

Figure 4. *Beam spreader* section, where the electron beam is directed into the different arcs after each pass of the linac.

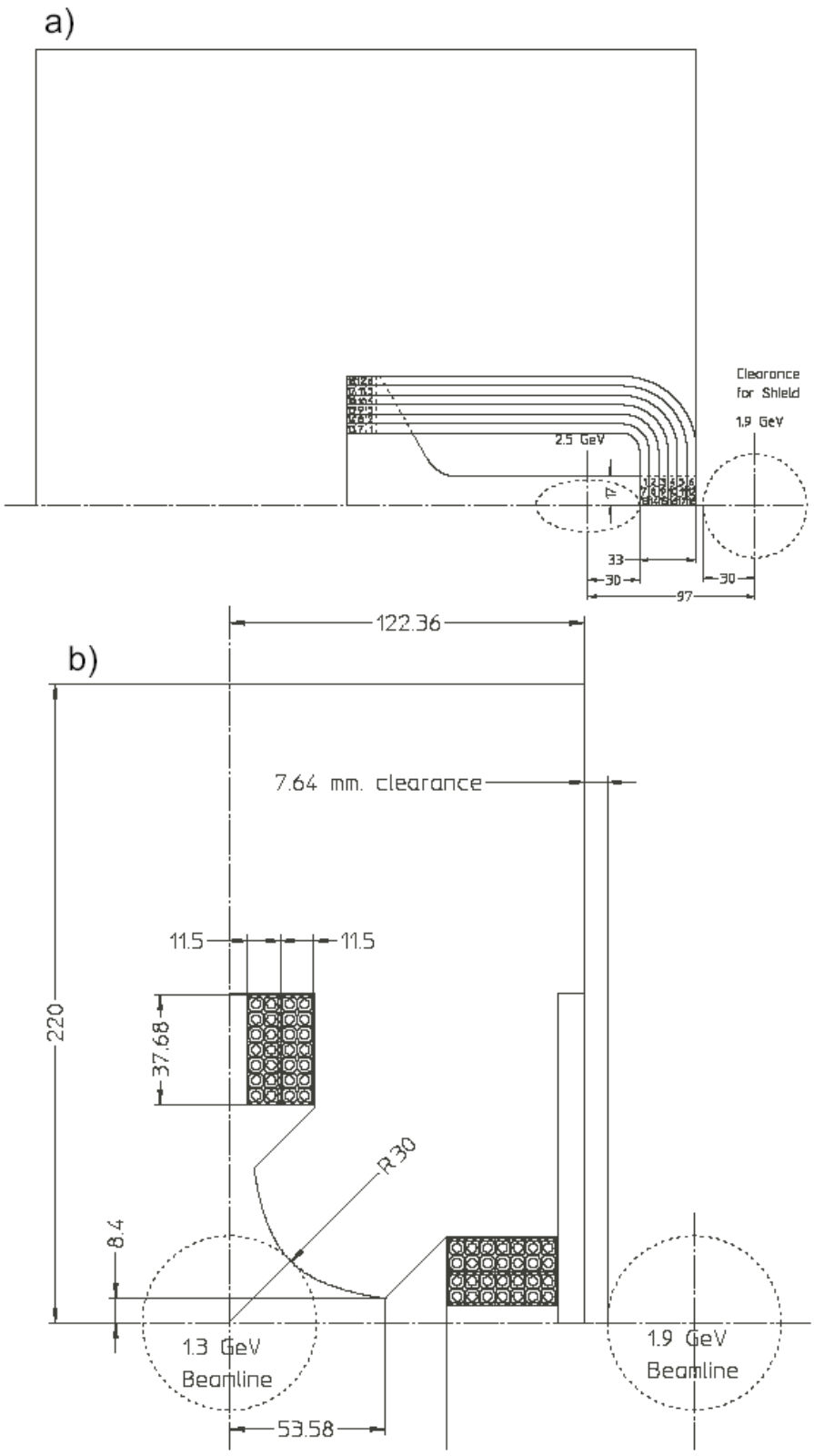

Figure 5. A crossections of a *beam spreader* septum bend magnet B3 (a) and a special quadrupole (b).

2.3 Magnetic arcs

All magnetic arcs have similar lattice. They transport the electrons of different energies from the end of the linac to the correspondent straight sections (or photon production section in the case of the arc 4) and back to the beginning of the linac. All arcs are comprised of three ~120° betatron phase advance cells each containing a string of bending magnets, three quadrupoles and three sextupoles. The third cell of each arc is used for matching of the arc's optical functions to the optical functions in the straight sections. The electron beam transport from the end of the linac to the beginning of straight sections is achromatic and isochronous. However, changes in the time-of-flight parameter (R_{56} matrix coefficient) can be easily adapted should electron bunch length adjustment be required at various stages of acceleration (and deceleration). Sextupoles are used to compensate chromaticity and second order terms affecting isochronicity. Bending magnets, quadrupoles and sextupoles that are used in the lattice of different arcs are mechanically identical.

2.4 Straight sections

All straight sections have a simple FODO lattice containing two identical beta-matching parts at two ends and a *tune trombone* in the middle. *Tune trombone* consists of four cells. With just two knobs, the variation of the betatron tunes can be made in a wide range of approximately ±0.5. The center section in Figure 3 shows typical beta-functions in the straight section.

2.5 Photon production section

Figure 6 shows beta and dispersion functions of the ring 4. The central part of this plot is the photon production section, which has six triple bend achromat cells with an arc angle of 6º per cell. The vertical and horizontal betatron phase advances per cell are π and 1.8 π. All cells begin and end in the middle of a short straight section, whose length is sufficient to host a 2 m long undulator. The vertical and horizontal beta-functions in the center of the undulator are 2.5 m and 7.5 m. The magnetic field of a central bend of a cell is 2 T, so it can be used as a source of hard x-rays. The vertical and horizontal beta-functions in this bend are 1.73 m and 3.4 m and the dispersion function is 6 cm. A 3.9 GHz rf structure operating at the first dipole mode is located between the arc and the photon production section. The vertical beta-function there is raised to 90 m. This helps to get an efficient time-dependent rf orbit kick needed for x-ray bunch compression [Ref.5]. The transfer matrix between this rf structure and similar place at the other end of the photon production section is made as the unit transfer matrix in both planes.

Due to the relatively low electron beam energy the effect of a synchrotron radiation on the electron beam is practically negligible. Even at 2.5 GeV the average energy loss of electrons in the undulator farm is approximately 500 keV and the increase of the energy spread due to quantum fluctuations of synchrotron radiation is approximately 50 keV, this is well below the beam energy spread of 200 keV of the incoming beam.

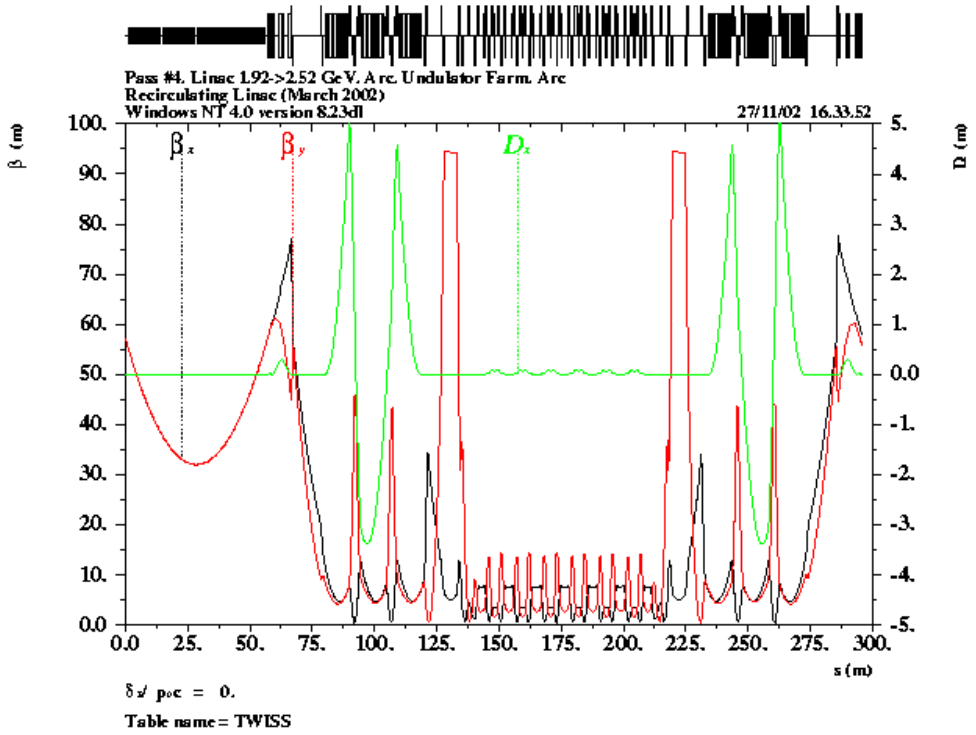

Figure 6. Lattice functions for ring 4 from entrance of the main linac through the arc, the photon production section, another arc and back to the linac. In a base line design, the arc returning the beam to the linac will not be built, and the beam will be taken to a dump.

3. Tracking studies

The single particle dynamics in the recirculating linac has been studied using the code COSY INFINITY [Ref. 4]. This code is perfectly suited for this task. It uses the Taylor series map that allows fast tracking and provides readily available parameter dependence between different quantities of interest. At the same time the deviation from symplecticity caused by truncation in the Taylor series is not important in a single pass system like a recirculating linac.

First we studied the path length difference for electrons propagating a single arc. A typical result is shown in Figure 7 for arc3 (the arc of the third ring). Figure 7 shows histograms for a spread of pathlengths before (red colour) and after (green colour) sextupole correction. Although FWHM of the histogram before sextupole correction is small (~10 fs), the tail extends to ~ 200 fs, which is undesirable. This is caused by second order time-of-flight terms in the lattice map. The sextupoles effectively reduce these terms such that the tails are confined within 50 fs as demonstrated in Figure 5b. It has been verified that the impact of the sextupoles on beta-functions, betatron phase advances and off-momentum orbit is insignificant.

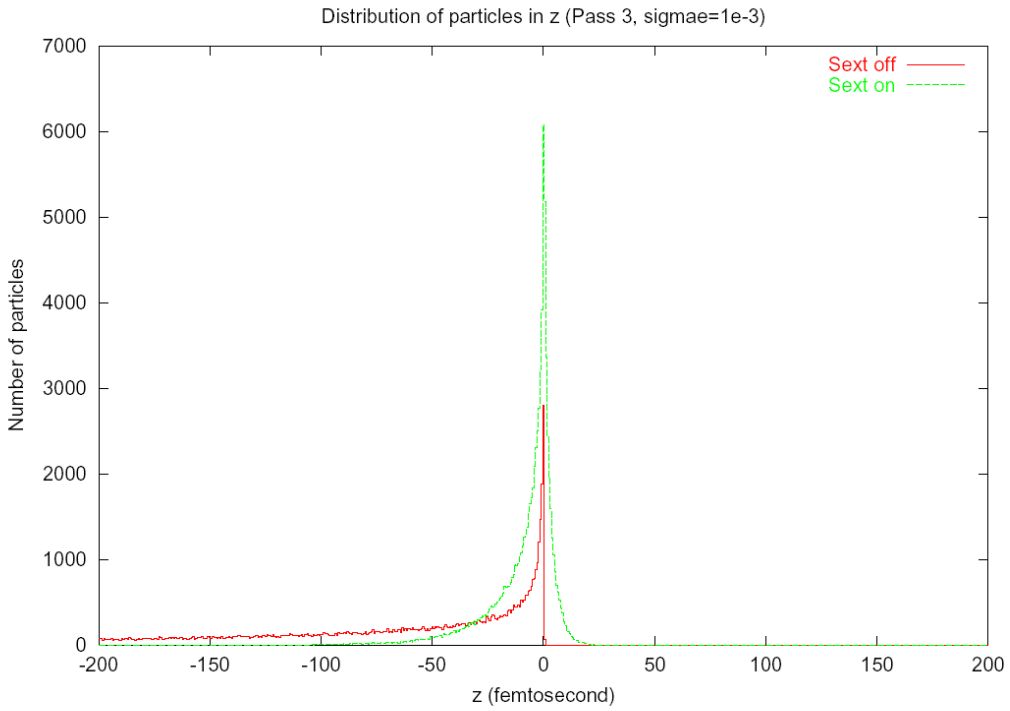

Figure 7. Histograms for a spread of pathlengths before (red colour) and after (green colour) sextupole correction.

Second, we study the effect of the lattice errors. So far only random static errors given in Table 1 were included and the BPMs errors were not considered. Table 1 also specifies beam parameters used in the tracking studies. In this study we found that alignment errors may cause vertical orbit distortions of the order of few millimeters. Then the orbit that goes off-set in the sextupoles induces a large coupling between horizontal and vertical planes. This is seen in few seeds in Figure 8 that shows vertical beam profile at the end of the arc3. Yet when stirring magnets were used to bring the beam offset down to ~200 μm, then the vertical beam size had typically shrunk to a few percent difference from the nominal one. The exception was found in one seed, where in addition to orbit correction we needed to re-optimize the strength of the sextupoles in order to get the normal beam size.

Table 1: Beam parameters and errors. All quantities are the rms values.

	Beam Parameters
Horiz. emittance (normalized, π mm mrad)	20
Vert. emittance (normalized, π mm mrad)	0.4
Momentum spread	1e-3
	Errors[*)]
Tilt (mrad)	0.2
Misalignment in x (μm)	150

Misalignment in y (μm)	150
Misalignment in z (mm)	1
Setupole field in bend magnets	b_3/b_1 = 1e-4 at r = 3 cm
Sextupole field in quadrupoles	b_3/b_2 = 1e-4 at r = 5 cm
Setting errors for all magnets	$\Delta B/B$ = 1e-3

*) For all errors we assume Gaussian distribution truncated at 2.5σ.

In order to do global tracking of the entire machine a simulation toll was developed based on symplectic integration. This code is designed using a concept of fiber bundles such that the fundamental component of a "beam line" is the discretized variable *s* on which physical data is attached as well as the geometrical transformations connecting the world of an individual magnet to the external world at that particular *s*. This allows us to handle recirculation of particles with different energies through common elements having them described in the lattice just once.

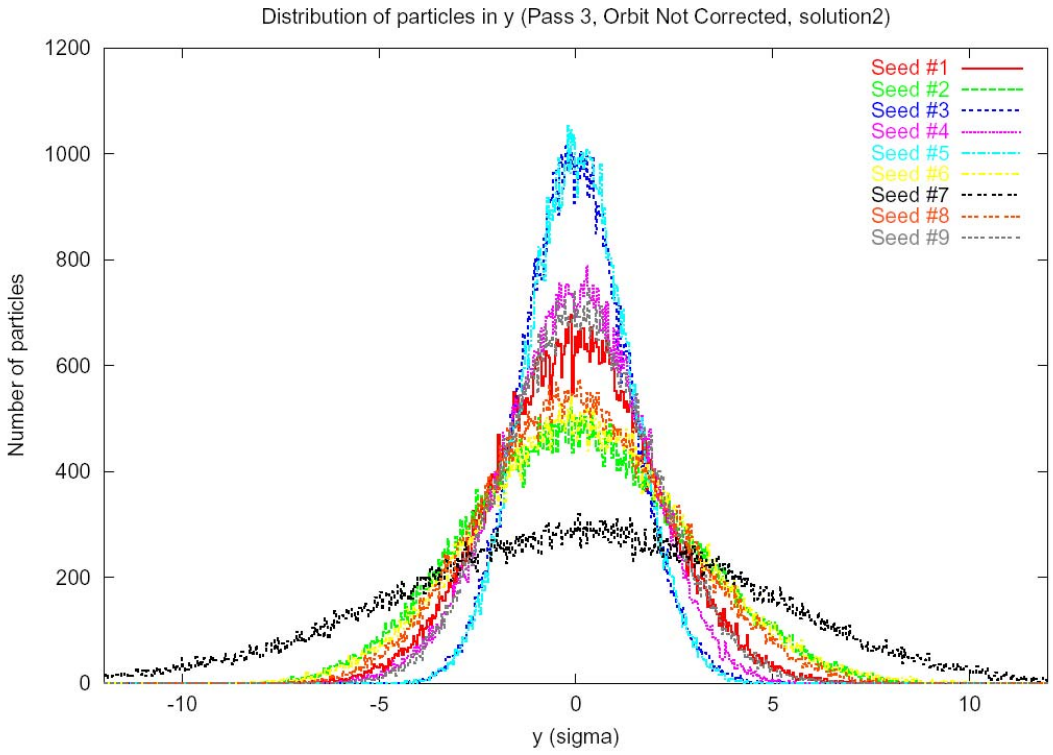

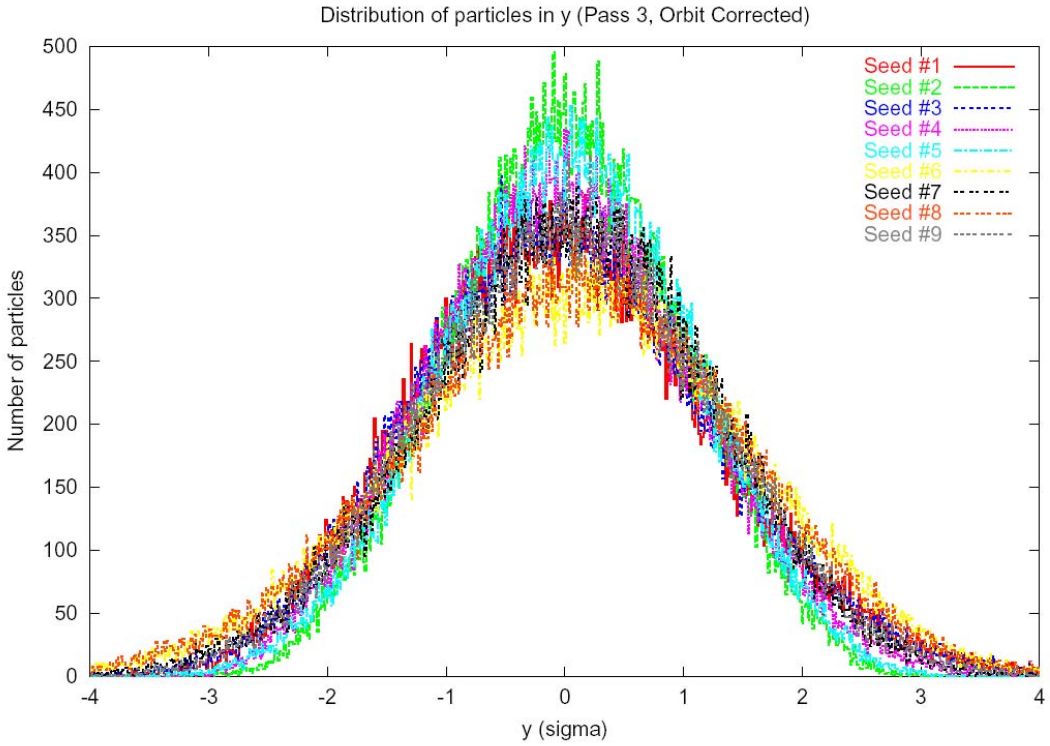

2. Summary

Lattice of the recirculating accelerator has been designed that meets all requirements for the femtosecond x-ray source. A design permits a tunability of the time-of-flight parameters, betatron phase advances, chromaticity over the different components of the lattice. The photon production section has been designed with six identical cells with variable beta-functions at the undulator and bend magnet x-ray source points. Tracking studies indicate that lattice design is insensitive to errors in magnetic field quality, but needs beam based alignment in case of an alignment errors. Detailed studies and simulations of a beam-based lattice tuning technique for machine commissioning are planed.

Acknowledgement. We are grateful to J. Corlett, I. Reichel, R. Wells, A. Wolski for useful discussions and P. Luft and D. Reavill for a help with the layout drawings.

References

1. J. Corlett et.al., "*A recirculating linac based synchrotron light source for ultrafast x-ray science*", proceedings of EPAC, Paris, 2002.
2. TESLA Technical Design Report, DESY 2001-011, March 2001.
3. A. Zholents et. al., "*Initial lattice studies for Berkeley femtosecond x-ray light source*", proceedings of EPAC, Paris, 2002.
4. M. Berz, NSCL Technical Report MSUCL-1088, Michigan State University, 1998.

Attachment

The list of all bending magnets showing the length of the magnet, number of magnets of the same kind, and magnetic field.

NAME	Number	L, m	H, T
BCH1	2	0.20	0.6400
BCH2	2	0.20	-0.6400
BCH3	2	0.20	-0.6400
BCH4	2	0.20	0.6400
BCH5	1	0.20	-0.6400
B0	2	0.82	1.1380
B1	2	0.82	-1.1380
B2	2	0.81	1.1380
B3	2	0.80	-1.1380
B4	2	0.80	1.1380
BA	138	0.75	1.1121
BU	12	0.20	0.9541
BU1	6	0.25	2.0000
BA0	3	1.26	0.3336
Total	**175**		

The list of all quadrupole lenses showing the length of the lens, number of lenses of the same kind, and the gradient of the magnetic field.

NAME	Number	L, m	G, T/m
Q41	2	0.3	8.6442
Q42	2	0.3	-8.2252
Q43	2	0.3	6.4036
Q44	2	0.3	-6.1269
QA41	4	0.6	9.3083
QA42	4	0.6	-9.2098
QA43	4	0.6	8.2946
QM1	2	0.6	-12.0904
QM2	2	0.6	9.2596
QM3	2	0.6	0.0000
QM4	2	0.6	0.0000
QM5	2	0.6	2.5914
QM6	2	0.6	-4.1391
QM7	2	0.6	-7.8992
QM8	2	0.6	16.6001
QM9	2	0.6	-8.5900
QM10	2	0.6	14.9142
QM11	2	0.6	-14.5071
QM12	2	0.6	10.6537
QU1	12	0.6	10.9304

NAME	Number	L, m	G, T/m
QS33	5	0.3	-6.3358
QS34	4	0.3	5.1885
QS35	2	0.3	-4.3479
QS36	2	0.3	4.7275
Q21	2	0.3	8.9132
Q22	2	0.3	-12.3582
Q23	2	0.3	10.5238
Q24	2	0.3	-14.3021
QA21	4	0.3	15.9172
QA22	4	0.3	-14.1934
QA23	4	0.3	15.4638
QS21	2	0.3	-5.1010
QS22	2	0.3	7.5878
QS23	5	0.3	-4.6920
QS24	4	0.3	4.2663
QS25	2	0.3	-3.0266
QS26	2	0.3	3.0069
Q11	2	0.3	3.5798
Q12	2	0.3	-7.4101
Q13	2	0.3	-0.2824

QU2	12	0.6	-14.6692
QU3	12	0.6	12.5153
Q31	2	0.3	7.7730
Q32	2	0.3	-10.5806
Q33	2	0.3	7.3114
Q34	2	0.6	-10.7737
QA31	4	0.3	16.4099
QA32	4	0.3	-16.9435
QA33	4	0.3	16.8483
QS31	2	0.3	10.9322
QS32	2	0.3	-7.9433

Q14	2	0.3	4.0941
QA11	4	0.3	11.2209
QA12	4	0.3	-8.3638
QA13	4	0.3	8.9432
QS11	2	0.3	2.8715
QS12	2	0.3	-2.6210
QS13	5	0.3	2.0994
QS14	4	0.3	-1.9434
QS15	2	0.3	3.5202
QS16	2	0.3	-1.5875
Total	**191**		